Water-soluble chlorophyll-binding proteins from Brassica oleracea allow for stable photobiocatalytic oxidation of cellulose by a lytic polysaccharide monooxygenase

N. Dodge
Kobenhavns Universitet

D. A. Russo
Friedrich-Schiller-Universitat Jena

B.M. Blossom
Kobenhavns Universitet

R.K. Singh
Kobenhavns Universitet

B. van Oort
Vrije Universiteit Amsterdam

R. Croce
Vrije Universiteit Amsterdam

M. J. Bjerrum
Kobenhavns Universitet

Poul Erik Jensen (✉ peje@food.ku.dk)
University of Copenhagen   https://orcid.org/0000-0001-6524-7723

Research

Abstract

Background

Lytic polysaccharide monooxygenases (LPMOs) are indispensable redox enzymes used in industry for the saccharification of plant biomass. LPMO-driven cellulose oxidation can be enhanced considerably through photobiocatalysis using chlorophyll derivatives and light. Water soluble chlorophyll binding proteins (WSCPs) make it is possible to stabilize and solubilize chlorophyll in aqueous solution, allowing for *in vitro* studies on photostability and ROS production. Here we aim apply a WSCP-Chl *a* as a photosensitizing complex for photobiocatalysis with the LPMO, *Tt*AA9.

Results

We have in this study demonstrated how WSCP reconstituted with chlorophyll *a* (WSCP-Chl *a*) can create a stable photosensitizing complex which produces controlled amounts of H_2O_2 in the presence of ascorbic acid and light. WSCP-Chl *a* is highly reactive and allows for tightly controlled formation of H_2O_2 by regulating light intensity. *Tt*AA9 together with WSCP-Chl *a* shows increased cellulose oxidation under low light conditions, and the WSCP-Chl *a* complex remains stable after 24 hours of light exposure. Additionally, the WSCP-Chl *a* complex demonstrates stability over a range of temperatures and pH conditions relevant for enzyme activity in industrial settings.

Conclusion

With WSCP-Chl *a* as the photosensitizer, the need to replenish Chl is greatly reduced, enhancing the catalytic lifetime of light-driven LPMOs and increasing the efficiency of cellulose depolymerization. WSCP-Chl *a* allows for stable photobiocatalysis providing a sustainable solution for biomass processing.

Background

Renewable and sustainable energy resources are necessary to sustain human consumption and decrease our reliance on fossil fuels[1]. Solutions for this can be found in nature where biological pathways exist that can convert sunlight into energy-rich biomass. Plant and algal biomass are renewable and can provide sustainable fuel alternatives including bioethanol, biodiesel and biogas[2]. Besides providing biomass, photosynthetic organisms have also inspired the development of photobiocatalysis, a biomimicry tool, designed to speed up enzymatic reactions using light[3−5]. Photobiocatalysis has been shown to increase the activity of cytochrome P450s[6], methane monooxygenases (pMMO)[7] and fungal lytic polysaccharide monooxygenases (LPMOs)[8−10].

LPMOs are soluble copper-enzymes, found in fungi, bacteria and insects, among others, that aid in the natural decomposition and recycling of biomass[11]. Their copper active site is solvent exposed and

coordinated by a histidine brace[12]. The flat binding surface and aromatic residues flanking the active site allow LPMOs to bind and cleave recalcitrant substrates such as chitin and cellulose[12]. These enzymes are therefore used in current industrial enzyme cocktails to increase saccharification efficiency and glucose release[13]. LPMOs have proven particularly useful at higher substrate loadings by synergistically enhancing the hydrolytic activity of cellulases[14,15].

For their catalytic cycle, LPMOs require an external reductant[16] and one of two cosubstrates, molecular oxygen (O_2) or hydrogen peroxide (H_2O_2)[17]. The cosubstrates interact with a reduced copper active site forming a reactive intermediate which can then oxidize the substrate. Recent studies have demonstrated significantly higher product yields when H_2O_2 is involved in LPMO catalysis[18,19]. However, the amount of H_2O_2 has to be controlled as high concentrations have been shown to be detrimental to LPMO activity[17].

The first report of light-driven LPMOs by Cannella *et al.*, demonstrated that LPMOs can also be light-driven[8]. This work proposed that the enhanced light-driven LPMO activity is due to a photoactivated electron transfer from a photosynthetic pigment directly to the LPMO. However, recent evidence indicates the formation of H_2O_2 by a photosensitizer is involved in the acceleration of light-driven LPMO catalysis[9,10]. Regardless of the exact mechanism, it is certain that photobiocatalysis has the potential to provide more powerful, faster and thus ´greener´ redox reactions[20].

Although photobiocatalysis is a relatively new field, photosensitizers have been used in a variety of applications, and tend to follow two main photodynamic mechanisms in the presence of oxygen[21]. Type I is electron transfer, where excited sensitizers can reduce oxygen resulting in superoxide (O_2^-), whereas Type II involves energy transfer producing singlet oxygen ($^1O_2$)[22]. Amongst the different photosensitizers it is common to find porphyrin ring-structured molecules, such as in chlorophyll (Chl) and its derivatives. However, the utilization of Chl in an industrial setting is challenging. Although chlorophyll molecules are quite stable within their native environment, in protein complexes of the thylakoid membrane, in an aqueous solution Chl molecules are highly insoluble and become more prone to photooxidation.

One way to stabilize Chl in solution is through reconstitution with water soluble chlorophyll-binding proteins (WSCPs). These soluble proteins form tetrameric complexes with Chl and have been shown to considerably increase photostability. Typically, Chl binding proteins are hydrophobic, membrane bound complexes, such as reaction centers and light-harvesting complexes involved in photosynthesis[23]. These proteins protect Chl from photooxidation with the presence of carotenoids. WSCPs however, do not contain carotenoids, but have been shown to have a similar photostabilizing effect on Chl. Although their biological function remains largely unknown, WSCP is the only known soluble Chl binding protein found in higher plants[24]. WSCP complexes have shown no involvement in photosynthesis, however, the cytosolic formation of reactive oxygen species could indicate a role in protection against pathogen attack[25]. Furthermore, these proteins have been localized in the endoplasmic reticulum bodies, only found in *Brassicaceae* plants, and thought to be involved in the stress response and injury[26]. It is believed

that WSCPs are able to stabilize the chlorophyll by creating a physical barrier, shielding the phytyl chain and magnesium ion from the surrounding solution and oxidative damage[27].

It has previously been shown that WSCP-Chl *a* complexes remain functional after prolonged incubation at high temperatures, as well as at extreme pH-values, suggesting potential for industrial use[24]. Therefore, in this work we propose to utilize WSCPs to bind Chl and prolong photosensitizer lifetime and, consequentially, activity of a light-driven LPMO system. To this end, a 22 kDa WSCP was reconstituted with chlorophyll *a* and the WSCP-Chl *a* complex was tested as a photosensitizer for light-driven activity of *Tt*AA9 LPMO from *Thielavia terretris*. The stability of the complex, and its ability to drive the LPMO, was tested under various light, temperature and pH conditions to demonstrate the robustness of the WSCP-Chl *a* complex.

Results

Stability of WSCP-Chla versus free Chl **a**

One of the central aims of photobiocatalysis is to use light to drive enzymes that catalyze reactions of interest such as the degradation of recalcitrant substrates like cellulose. For application of light-driven systems, the lifetime of the photosensitizer is, therefore, vital to prolong the catalytic lifetime. The photostability of free Chl *a* and Chl *a* bound to the WSCP (WSCP-Chl *a*) was measured over time in an LPMO light-driven system which includes *Tt*AA9 and a reductant (ascorbic acid, Asc). Photostability is in this context defined as the loss of Chl fluorescence over time relative to initial fluorescence (F/F_0).

As expected, we observed that, in the light-driven LPMO system, the WSCP-Chl *a* complex is more stable than free Chl *a* in all conditions (Fig. 1a). When combined with *Tt*AA9 and Asc, WSCP-Chl *a* showed 76 ± 4% fluorescence after 1 h compared to Chl *a* where only 5 ± 0.2% remained. In the partial assay systems, ascorbic acid enhances the photostability of both the WSCP-Chl *a* complex and Chl *a*, whereas the presence of the *Tt*AA9 decreases the apparent photostability. However, when combining the *Tt*AA9 and Asc the negative effects caused by the enzyme seem to be counteracted for both WSCP-Chl *a* and Chl *a*. The final fluorescence ratio (F/F_0 at 60 min) was analyzed with single factor ANOVA. All WSCP-Chl *a* samples were significantly different from each other (p < 0.001).

Effect of light and temperature on the stability of WSCP-Chl **a** versus free Chl **a**

For application of photobiocatalytic LPMO reactions, the photosensitizer should ideally be stable under a broad range of temperatures. For example, several fungal LPMOs (AA9) have been shown to have the highest activity levels at temperatures ranging between 40−50 °C[34]. Therefore, photostability was tested at 25 °C and 50 °C. Together with temperature, light intensity was also varied to investigate which of the two factors has a larger influence on the photostability of the complex. Both photosensitizers were subjected to 50 and 200 µmol m^{-2} s^{-1} for 1 h at 25 and 50 °C (Fig. 1b). As expected, lower light conditions (50 µmol m^{-2} s^{-1}) were beneficial for both WSCP-Chl *a* and free Chl *a*. When the light was

increased to 200 µmol m^{-2} s^{-1}, a considerable loss in photostability was observed. The rise in temperature causes an extra 15% loss of fluorescence in free Chl a compared to only 5% in WSCP-Chl a complex.

Effect of pH on stability of WSCP-Chl a versus free Chl a

Many enzymatic reactions require rather acidic or basic environments. For example, LPMO containing enzyme cocktails have been shown to achieve a maximum depolymerization at pH 5[35,36]. Therefore, it is important that a photosensitizer remains stable across a broad range of pH-values. In order to determine the pH stability of the WSCP-Chl a complex and free Chl a, both were incubated in different buffers, ranging from pH 5−8, and their photostability was measured over time (Fig. 1c).

The photostability of WSCP-Chl a is unaffected by the changes in pH as there is no significant difference between all four samples with single factor ANOVA ($p > 0.05$). The stability of free Chl a is expected to be favored by high pH as these pigments are known to lose their central Mg ion in acidic conditions[37,38]. Although this effect is not seen under our experimental conditions, Chl a remains unstable with between 4−12% fluorescence remaining after 60 min under all conditions. WSCP-Chl a retained between 61−63% At pH 5−8.

Photostability of WSCP-Chl a *and Chl* a *after 24 hours*

A 24-hour assay was done at low light (50 µmol m^{-2} s^{-1}) to demonstrate the long-term stability of WSCP-Chl a (Fig. 1d). One phase decay model was used to approximate the half-life of both pigments with a confidence interval over 95%. Chl a shows a half-life of 1.43 hours while WSCP-Chl a is estimated at 23.34 hours.

Effect of light intensity on H$_2$O$_2$ production

In light of the recent publications suggesting H$_2$O$_2$ is a key factor in light-driven LPMO [9,39] we proceeded to investigate the light-driven formation/generation of H$_2$O$_2$ from WSCP-Chl a and free Chl a under varying light intensities (0, 50, 100, 200, and 500 µmol m^{-2} s^{-1}) (Fig. 2a).

With WSCP-Chl a, higher light intensities lead to a faster rate of H$_2$O$_2$ formation, as measured by the Ampliflu™ assay, with a maximum value of 298 µM after 30 min in 500 µmol m^{-2} s^{-1} light. The highest H$_2$O$_2$ formation seen in free Chl a is at 200 µmol m^{-2} s^{-1} with a total of 60 µM H$_2$O$_2$ after 30 min. In the absence of light, no formation of H$_2$O$_2$ is observed. Interestingly, Chl a exposed to a light intensity of 500 µmol m^{-2} s^{-1} also showed no formation of H$_2$O$_2$. This is likely a result of rapid photobleaching of Chl a. To establish the correlation between light intensity and H$_2$O$_2$, the time traces in Fig. 2a were each fitted with a linear function. The resulting slopes correspond to the rate of H$_2$O$_2$ measured per minute (Fig. 2b).

Effect of reductant concentration and light on H_2O_2 formation

After having determined the correlation between light intensity and H_2O_2 formation, we investigated the effects of the reductant (Asc) concentration on H_2O_2 formation. The assay was set up with WSCP-Chl a and four different concentrations of Asc (0, 250, 500, and 1000 µM) (Fig. 2c). Higher concentrations of Asc led to greater endpoint H_2O_2 formation, however, 1000 µM Asc forms similar concentrations of H_2O_2 as 250 µM Asc after 10 min. H_2O_2 levels were below the detection limit in the absence of Asc (0 µM), indicating the necessity of reductant in the light-driven mechanism. With 1000 µM Asc, the addition of TtAA9 reduces amount of detected H_2O_2 to that in the absence of Asc, suggesting that either TtAA9 prevents the formation of H_2O_2, or, more likely, that TtAA9 degrades H_2O_2 that is formed before it can react with Ampliflu™. In order to demonstrate the tight control of H_2O_2 production by WSCP-Chl a, a light-dark alternating assay was performed. In this assay, WSCP-Chl a was placed in 50 µmol m^{-2} s^{-1} for 5 min followed by 5 min of fluorescence measurements in the dark (Fig. 2d). This assay clearly demonstrates the light-dependence of H_2O_2 production by WSCP-Chl a. Once again, this assay also shows the importance of Asc in the system for H_2O_2 production.

Light-driven Tt **AA9** activity assays

To assess whether the higher photostability of the WSCP-Chl a would lead to higher TtAA9 product formation, light-driven activity assays were performed with TtAA9 using varying concentrations of reductant. Since high concentrations of H_2O_2 can be detrimental to LPMO activity[18,40], and the WSCP was shown to be more stable at lower light intensities (Fig. 1b), the light intensity was reduced to 100 µmol m^{-2} s^{-1} for TtAA9 experiments. Subsequently, the optimization process was focused on the "feed rate" of Asc to control the H_2O_2 production in the assays. The feed rate is defined as the concentration (mM) of Asc added at certain time intervals (min). It is difficult to determine the necessary reductant concentration since there are many factors involved. To demonstrate the importance of reductant concentrations, three assays with varying Asc feed rates: 2 mM Asc every 60 min (Fig. 3a), 1 mM Asc every 60 min (Fig. 3b), and 500 µM every 20 min (Fig. 3c), with gluconic acid concentrations measured every 20 min for 2 hours.

In Fig. 3a, in the presence of 2 mM Asc, all samples show high activity in the first 20 min, after which activity halts. Final concentrations were 61, 39, and 56 (mg L^{-1}) for samples WSCP-Chl a, free Chl a, and no pigment, respectively. Upon halving the concentration of Asc and adding twice (1 mM/h), there is a noticeable increase in overall activity of all samples (Fig. 3b). After 80 min where we see a plateau in the assay with TtAA9 and Chl a. In the final assay (Fig. 3c), the concentration of Asc was changed to 500 µM, added every 20 min, which led to a significantly increased activity (p < 0.05; determined for t = 120 min) for both assays containing photosensitizers. TtAA9 with WSCP-Chl a resulted in a final gluconic acid

concentration of 110 (mg L^{-1}). Chl a also boosted to activity TtAA9 significantly with 75 mg L^{-1} compared to TtAA9 alone at 59 mg L^{-1}.

High-Performance Anion-Exchange Chromatography (HPAEC)

The slightly acidic nature of carbohydrates allows for highly selective separations using anion exchange at high pH. The C1-oxidized products are easily characterized as seven distinct singular peaks just prior to the jagged elution of the C4 oxidized products (Fig. 4).

For this study, the chromatograms can be used to compare the relative signal intensities of the oxidized products in in the different samples. TtAA9 activity after 3 hours with WSCP-Chl$a$ and shows a max signal intensity of 168.8 (nC) at 22 min corresponding to cellotetraonic acid (Glc$_3$Glc1A). TtAA9 + Chl a and TtAA9 on its own also demonstrate max intensities with Glc$_3$Glc1A at 115.31 and 81.2 (nC), respectively (Fig. 4). A control containing WSCP-Chl$a$ with no TtAA9 shows no C1 oxidations peaks the visible cellobiose (Glc$_2$) is background from the substrate. The area under the C1 oxidation peaks was used to estimate the photobiocatalytic enhancement. The area for TtAA9 + Chl a was 1.88x than TtAA9 alone, while TtAA9 + WSCP-Chl a was 3.4x greater compared to TtAA9 alone.

Discussion

Most biological pigments, and in particular chlorophyll, are prone to rapid photooxidation if exposed to light outside of their natural environment. Due to this, the use of biological pigments in photobiocatalysis is still limited. Therefore, for future application, it is of interest to describe novel pigment systems capable of withstanding the, potentially, harsh biomanufacturing conditions. The work reported here presents WSCP-Chl a as a possible candidate for industrial application of chlorophyll-based photosensitizers. Through the controlled light-induced formation of H$_2$O$_2$, it was possible to adjust conditions to obtain increased TtAA9 activity. Overall, TtAA9 activity was enhanced over 3-fold and confirmed using various LPMO activity detection methods.

Photostability Assays

The WSCP-Chl a complexes were tested under various conditions to confirm the photooxidative protection properties of the WSCP[23,24]. The tested conditions included individual and combinations of enzymatic activity assay components including TtAA9 and Asc. Most notably we observed a decreased photostability in the WSCP-Chl a complex as well as the free Chl a caused by the presence of TtAA9 with (Fig. 1a). However, Asc appears to counteract this negative side effect most likely due to its antioxidant properties. This was seen by the restoration of photostability in both WSCP-Chl a and free Chl a when TtAA9 and Asc are combined.

Light and temperature effects were also tested on both WSCP-Chl a and Chl a. Overall improvement of photostability is seen in all conditions for both WSCP-Chl a and Chl a since the light intensity is lowered considerably. At 500 µmol m^{-2}s^{-1}, with pigment alone, WSCP-Chl a retained 56 ± 1.8% fluorescence after 60 min, compared to 61.2 ± 1.1% and 87.9 ± 4% at 200 and 50 µmol m^{-2}s^{-1}, respectively. Chl a shows some improvement from 4.6 ± 1.3% at 500 µmol m^{-2}s^{-1}, to 29.1 ± 0.6% and 43.9 ± 3.5% at 200 and 50 µmol m^{-2}s^{-1}, respectively. As expected, light intensity has a bigger influence on photostability than temperature (Fig. 1b). Temperature is important for the activity of the LPMOs as most assays are performed at 45–50 °C [41]. The loss of 4.5% photostability is minimal at 50 °C when considering the overall goal is increased activity of TtAA9. Another important factor for activity assays is pH. LPMO assays are generally performed around pH 5-7[41]. The WSCP-Chl a showed no change in photostability between pH 5–8 (Fig. 1c). In order to demonstrate the long-term stability of WSCP-Chl a, a 24 hour assay was run at 50 µmol m^{-2}s^{-1} (Fig. 1d). Lifetimes were estimated using a one phase decay model. WSCP is estimated to increase pigment half-life 16-fold from 1.43 hrs to 23.34 with WSCP-Chl a.

H$_2$O$_2$ Assays

WSCPs bound to Chl have been shown to produce large amounts of ^{1}O$_2$*[27]. It has also been demonstrated that Asc reacts with ^{1}O$_2$* to form H$_2$O$_2$[42]. In context of LPMOs, H$_2$O$_2$ has been shown to increase LPMO activity in several instances[9,16,43]. That being said, H$_2$O$_2$-driven LPMO catalysis has two sides. In order to increase activity, the concentration of H$_2$O$_2$ has to be optimal for the LPMO to function. High concentrations lead to self-inactivation of non-substrate bound LPMOs[19]. In an attempt to determine the rate of H$_2$O$_2$ produced by WSCP-Chl a with Asc, several assays were performed under varying light conditions. Higher light intensities led to greater H$_2$O$_2$ formation as seen in Fig. 2a. As long as there is Asc present in the reaction, then formation of H$_2$O$_2$ is expected to increase continuously until the pigments are degraded. However, the rate of H$_2$O$_2$ generation does not increase linearly with light intensity (Fig. 2b). These results can be used to adjust the light intensity for an estimated production of H$_2$O$_2$ µM/min. However, the exact value is difficult to estimate due to the fact that Asc is also involved in scavenging H$_2$O$_2$[44]. As seen in Fig. 2c, higher concentrations of Asc do not necessarily lead to more H$_2$O$_2$ initially. There appears to be competition between formation and scavenging reactions by Asc. H$_2$O$_2$ is able to oxidize Asc as well as resulting oxidation products such as dehydroascorbic acid and 2,3-diketoguloric acid[45]. Despite the competing reactions, H$_2$O$_2$ formation remains tightly controlled under light and dark incubation as seen in Fig. 2d. This reaction is unmistakably dependent on Asc and light.

LPMOs have been shown to consume H$_2$O$_2$ in the presence of substrate[17], which is also the case with 1000 µM Asc in the presence of TtAA9 where negligible amounts of H$_2$O$_2$ are detected throughout course of the experiment (Fig. 2c). In order to test LPMO consumption of H$_2$O$_2$, TtAA9 was combined with 1 mM Asc. Very little to no accumulation of H$_2$O$_2$ is seen after 30 min, comparable to that seen in the control with 0 mM Asc added. This supports the idea that LPMOs possess peroxygenase activity. During longer

assays times, Asc is added in intervals[46] to keep the reaction going (Fig. 3). By controlling reductant concentration, we can limit the accumulation of H_2O_2 over time. This has been shown to work with LPMOs by adding lower concentration of H_2O_2 and reductant more often yielding higher productivity. Concentrations over 100 µM H_2O_2 have been shown to lead to enzyme inactivation[17,19,46].

Light-driven Tt **AA9** Activity Assays

Two different methods were used for determining *Tt*AA9 activity: gluconic acid estimation and detection of C1 and C4 oxidized products by HPAEC-PAD. Gluconic acid assays were used to quantify C1-oxidions of *Tt*AA9 as this is the primary function of Type I LPMOs. Figure 3a, at 2 mM Asc, shows inactivation after 20 min in both *Tt*AA9 and *Tt*AA9 with Chl *a*, with some increase in activity *Tt*AA9 with WSCP-Chl *a*. In Fig. 3b we estimated a concentration of 123 µM H_2O_2 after 20 min with 1 mM Asc. In Fig. 3a, it would then be expected that there is at least 200 µM H_2O_2 produced by WSCP-Chl *a* after 20 min. This could potentially explain why some light-driven samples appear to hinder TtAA9 productivity. Previous reports have shown that while low concentrations of H_2O_2 are beneficial, high concentrations can be detrimental to LPMOs and lead to enzyme inactivation. Adding 500 µM every 20 min leads to improvement of activity in all samples (Fig. 3c), as expected when high concentrations of H_2O_2 are damaging to *Tt*AA9 activity. The signal intensities from the HPAEC confirm the light enhanced substrate oxidation, WSCP-Chl *a* with *Tt*AA9 is the most active, followed by Chl *a* with *Tt*AA9 and then *Tt*AA9 alone (Fig. 4). Similar results were seen for *Tt*AA9 with chlorophyllin and light[8].

Light-driven Formation of H_2O_2 with WSCP-Chl a

Cannella *et al.* hypothesized that upon light-excitation, pigments would become excited and then transfer an electron directly to the LPMO[8]. The LPMO would be reduced and could use O_2 to oxidize the substrate. The reductant, Asc or lignin, would be responsible for replenishing the donated electrons in the pigments, allowing for further excitation and electron transfer[8]. Based on data presented in this study, it seems more likely that H_2O_2 is involved in the catalytic enhancement of *Tt*AA9 when using WSCP-Chl *a* (Fig. 5). This is also in agreement with a recent study which also shows that H_2O_2 and O_2^- are involved in the light-driven reaction of LPMO and several chlorophyll derivatives[9]. A recent publication by Bissaro *et al.* (2020) utilized chlorophyllin to drive an LPMO producing large quantities of H_2O_2. Due to the stability of WSCP-Chl *a*, low light (50 µmol m^{-2}s^{-1}) and very little WSCP-Chl *a* (2.6 µM) are needed to produce enough H_2O_2 for successful photocatalysis of an LPMO[9]. For comparison, 50–100 µmol m^{-2}s^{-1} is measured as instantaneous photosynthetic photon flux density (PPFD) on a cloudy winter day in Northern Europe[47].

Conclusion

In this study, a recombinant WSCP from *Brassicaceae oleracea* var. bortrys (WSCP1), was reconstituted with chlorophyll a to form a stable tetrameric complex (WSCP-Chl *a*). WSCP-Chl a was then tested for

photostability under various conditions. These conditions were designed to test the use of this complex as a new photosensitizer for the emerging field of photobiocatalysis. The complex displayed superior stability under high light conditions, as well as varying pH and in combination with enzymatic assay components. It was further shown that in combination with Asc, WSCP-Chl a formed H_2O_2 when exposed to light. The hydrogen peroxide formation was dependent on both the reductant (Asc) concentration, as well as the light intensity. To test the use of this application of this new photosensitizer, WSCP-Chl a was combined with C1 oxidizing *TtAA9* to enhance hydrolytic activity upon light exposure. With the recent discovery of LPMO peroxygenase activity, it is proposed, that WSCP-Chl a can produce steady amounts of H_2O_2 upon light exposure which can in turn enhance LPMO activity. Light-driven assays yielded a 2 to 3-fold increase in activity which was confirmed using both gluconic acid determination and HPAEC chromatograms. Based on the data provided in this study, it is believed that WSCP-Chl a is promising addition to the field of photobiocatalysis.

Methods

Construct design and plasmid generation

The amino acid (AA) sequence of the mature WSCP1 protein (AA 20−218) from *Brassica oleracea var. botrytis* (UniprotKB: Q7GDB3) was custom synthesized by GenScript (USA) and inserted into the TOPO® cloning site of the pET151/D-TOPO® vector (Invitrogen) by overlap extension PCR[28]. The correct insertion of the gene was confirmed by Sanger sequencing (Eurofin Genomics) and the generated plasmid termed pDAR15. For all cloning steps, *E. coli* strain NEB® 5-alpha (NEB5α) (New England Biolabs Inc) was used. Plasmid amplification was done using QiaPrep Spin Miniprep Kit (Qiagen). Purified pDAR15 was stored at -20 °C. Transformed *E. coli* BL21 (DE3) was used for expression of WSCP1 (hereafter, WSCP).

Production of WSCP

E. coli BL21 (DE3) containing the pDAR15 plasmid was taken from a 20% glycerol stock incubated overnight at 37 °C on LB agar containing 50 µg mL^{-1} ampicillin. A single colony was used to inoculate 20 mL of LB media containing 50 µg mL^{-1} ampicillin and incubated overnight at 37 °C and 200 rpm. Subsequently, 500 mL of LB, containing 50 µg/ml ampicillin, were inoculated to a final OD_{600nm} of 0.05 and incubated (37 °C; 200 rpm) until an OD_{600nm} of 0.5 was reached. The culture was then induced with 1 mM isopropyl-β-D-thiogalactopyranoside (IPTG) for 4 h. The cells were harvested by centrifugation for 15 min at 3000 x g and pelleted cells were resuspended in 50 mL lysis buffer (50 mM NaH_2PO_4; 300 mM NaCl; 20 mM imidazole pH 7.8).

Purification of WSCP

E. coli BL21 (DE3) cells were lysed by using the CF1 Cell Disrupter (Constant Systems, Ltd.) at approximately 22 kPSI. The lysed sample was then centrifuged for 30 min at 4696 x g to remove cell debris. WSCP was purified with two rounds of His-tag affinity chromatography. Briefly, the lysate was

incubated for 1 h shaking (4 °C; 60 rpm) with Ni-NTA agarose beads. The beads were washed with 2 column volumes (CV) of each wash buffer containing increasing imidazole concentrations (50 mM NaH_2PO_4; 300 mM NaCl; 25, 50, and 60 mM imidazole, pH 7.8). WSCP was then eluted with 5 CV of elution buffer (50 mM NaH_2PO_4; 300 mM NaCl; 300 mM Imidazole). The eluted fractions were desalted using Amicon® Ultra centrifugal filters with a 10 kDa cutoff (Merck Millipore). The protein samples were buffer exchanged with 50 mM sodium phosphate (pH 7.8). Protein concentration was determined with a Nanodrop spectrophotometer (Thermo Scientific) using the mass attenuation coefficient (E1%; 11.31 L $g^{-1}cm^{-1}$). This was calculated using the molar attenuation coefficient (ε_{molar}; 28,420 M^{-1} cm^{-1}) and the molecular mass (M_r; 25,122 Da). These values were calculated from the amino acid sequence of 6xHis-WSCP using ExPASy ProtParam[29]. Protein purity was verified by sodium dodecyl sulfate-polyacrylamide gel electrophoresis (SDS-PAGE) and immunoblotting.

SDS PAGE and immunoblotting

Protein samples were incubated at 95 °C for 5 min with SDS-Loading buffer (50 mM Tris-HCl, pH = 6.8, 10% glycerol, 2% SDS, 100 mM DTT, 0.05% bromophenol blue) and separated on a 12% Criterion™ XT bis-tris pre-cast protein gel (Bio-Rad). All gels were run in 2-morpholinoethanesulfonic acid (MES) running buffer (Bio-Rad) at 180 V. After SDS-PAGE separation, the gels were either stained with Coomassie or immunoblotted. For immunoblotting, the proteins were transferred to a 0.2 μm polyvinylidene difluoride (PVDF) membrane using a Trans-Blot® Turbo Transfer System (Bio-Rad) for 7 min at 25 V. Afterwards the membranes were blocked for 1 h at RT with 5% skimmed milk powder (w/v) in phosphate buffered saline with 0.05% Tween-20 (PBS-T) buffer. The membrane was then incubated at 4 °C overnight with an anti-6X His primary antibody solution (1:100 dilution in PBS-T with 1% milk). The blot was then washed for 3 × 10 min with PBS-T and incubated with and anti-rabbit horseradish peroxidase-conjugated secondary antibody (1:5000) for 1 h at RT. The blot was rinsed (3 × 10 min with PBS-T) and developed using SuperSignal™ Chemiluminescent Substrate developer (Thermo Scientific) followed by immediate imaging (Fig. S1).

Chlorophyll extraction and purification

Chlorophyll a was extracted from the cyanobacterium *Synechococcus elongatus* UTEX 2973. The lyophilized cyanobacterial pellet was made into a fine powder using a pestle and mortar and resuspended in 100% methanol to extract pigments. The cell debris was spun down at 4000 x g for 10 min at 4 °C. The supernatant was removed using a MiniVac Evaporator (Labogene A/S, Denmark). Methanol extraction was repeated until the cyanobacterial pellet turned blue. The dried pigments were resuspended in 1:4 methanol:acetone and stored at -20 °C.

Thin Layer Chromatography (TLC) was used to separate the pigments on RP-18 F_{245}s silica gels. The TLC mobile phase was comprised of 7:11:1 acetone:methanol:ddH_2O mixture. A dark green band containing chlorophyll a (Fig. S2) was scraped off and dissolved in 100% acetone. The silica was then spun down at 5000 x g and the supernatant was removed and evaporated using a Spin-Vac. After removing the

acetone, the Chl *a* was resuspended in 96% ethanol (EtOH) and stored in the dark at -20 °C. The amount of Chl *a* was calculated using the ε_{molar} of 74,400 cm^{-1}M^{-1} [24].

WSCP-Chl a Reconstitution

Reconstitution was performed with a 5x molar excess of Chl *a* to WSCP for a fully saturated complex (i.e. 4Chl*a*:4WSCP)[24]. The Chl *a* solution was added dropwise to the protein solution to a final concentration of 20% EtOH. The mixture was incubated at RT for 30 min at 1000 rpm in the dark. The reconstitution mix was then buffer exchanged with 50 mM sodium phosphate buffer (pH 7.0) to remove excess EtOH with 30 kDa cutoff Amicon® Ultra centrifugal filters (Merck Millipore). The reconstitution mix was placed in a new microcentrifuge tube which was then centrifuged at 15000 x g for 10 min. The supernatant was removed and stored at 4 °C in the dark. Stoichiometry of the reconstituted complex was determined by measuring Chl *a* (673 nm) and WSCP (280 nm) absorbance using 10 mm quartz absorption cuvettes. Absorption spectra were measured between 250–750 nm and compared to published data (Fig. S3)[24].

Assay for Determination of Photostability

Chl *a* and WSCP-Chl *a* fluorescence was compared under various conditions using the Biotek Synergy™ microplate reader with Gen5™ Data Analysis Software. The fluorescence was measured at 420 nm and emission was integrated over 650–700 nm. Assays had a total volume of 200 μL and were performed in black 96-well Nunc™ optical plates (Thermo Scientific). Assay mix included *Tt*AA9 (0.035 mg mL^{-1}), ascorbic acid (1 mM) and Chl *a* or WSCP-Chl *a* (2.6 μM) (OD = 0.2, ε_{molar} of 74,400 cm^{-1}M^{-1}) calculated according to Palm *et al.*[24] and 50 mM sodium phosphate buffer (pH 6.3). Varying conditions included light intensity (50, 200, 500 μmol m^{-2} s^{-1}), temperature (25 and 50 °C) and pH (50 mM potassium phosphate buffer pH 5, 6, 7, 8). Illumination was with cool white LEDs (4000 K spectrum) in a customized light rig and powered by Velleman™ DC Lab Switching Mode Power Supply. All experiments were performed in triplicates and data shown are the averages with the standard error of the mean (SEM).

Assays for the determination of H_2O_2 production

The production of H_2O_2 in the light-driven assays was measured using Ampliflu™ Red (Sigma) according to Singh *et al.*[30]. All reactions were performed in black 96-well Nunc™ optical plates (Thermo Scientific). The assay was sampled every 10 min and 10 μL samples were mixed with 2 μL Ampliflu™ Red (5 mM stock), 15 μL Horseradish Peroxidase from Sigma (300 U mL^{-1}), 2 μL Ethylenediaminetetraacetic acid (EDTA) (10 mM stock), and 171 μL 50 mM K_2PO_4 (pH 6.0). Measurements were made on Biotek Synergy™ microplate reader preheated to 37 °C and analyzed with Gen5™ Data Analysis Software. Excitation was set to 557 nm and emission was measured at 583 nm with three replicate reads per reaction. A standard curve was made immediately after purchasing ≥30% H_2O_2 for trace analysis from Sigma Aldrich. Varying conditions included light intensity (0, 50, 100, 200, 500 μmol m^{-2} s^{-1}) and ascorbic acid (0, 250, 500, 1000 μM). All experiments were performed in triplicates and data shown are the averages with the standard error of the mean (SEM).

Light-driven assays

Activity assays were performed using *Tt*AA9 from Novozymes A/S. Purification and copper loading of *Tt*AA9 was performed according to Singh *et al.*[30]. From a stock solution of 7 mg mL^{-1}, a final concentration of 0.035 mg mL^{-1} *Tt*AA9 was used in each assay. The substrate stock was 0.5% w/v cellulose nanofibrils (CNF) with a final concentration of 0.25% w/v used in all assays. 50 mM sodium phosphate (pH 6.3) was used in all assays and the reductant ascorbic acid (Asc) was purchased from Sigma Aldrich and aliquoted in 200 mM stock solutions and kept at -20 °C. The detergent, n-Dodecyl-β-D-Maltoside (β-DM) was kept at -20 °C in 2% stock solutions and 0.03% in assays. This was used to keep Chl *a* soluble for control assays. Assays were carried out at either 25 or 50 °C using an Eppendorf Thermomixer while mixing at 1000 rpm. Samples were filtered using 0.22 µm MilliporeSigma™ MultiScreen$_{HTS}$ Durapore™ 96-well plates (Fischer Scientific) immediately after the assay completion. This removes the substrate from the reaction, stopping further catalysis by *Tt*AA9.

Gluconic Acid Determination

The soluble fraction of CNF treated with *Tt*AA9 was incubated overnight at 40 °C with 8 µg mL^{-1} ß-glucosidase from *Aspergillus niger* (Megazyme Cat. No. E-BGLUC w/ 50 U mg^{-1}). This leads to the hydrolysis of terminal, non-reducing β-D-glucosyl residues with release of β-D-glucose and gluconic acid (C1-oxidation product)[31]. Gluconic acid is then determined using the D-Gluconic Acid/D-Glucono-δ-lactone Assay Kit from Megazyme, following manufacturer's instructions for a microplate assay. Absorption was measured using Biotek Synergy™ microplate reader at 340 nm. All experiments were performed in triplicates and data shown are the averages with the SEM.

Oligosaccharide production analyzed by HPAEC-PAD

High-Performance Anion Exchange Chromatography (HPAEC) was used to analyze released oligosaccharides after LPMO-driven cellulose oxidation. HPAEC was performed on Dionex™ ICS-5000 + with a PAD detector from Thermo Scientific. A CarbonPac PA1 column (two 2 × 50 mm guard columns followed by a 2 × 250 mm analytical column) was run with a flow rate of 0.25 mL min^{-1} at 30 °C. The aldonic acids were separated chromatographically as previously described[32]. The elution gradient was (Eluent A: 0.1 M NaOH; Eluent B: 1M NaOAc in 0.1 M NaOH): 100% A:0% B to 90% A:10% B (10 min), then to 83.1% A:16.9% B (25 min) and lastly 0% A:100% B (30 min). For reconditioning of the column 100% A:0% B was applied for 15 min (35–50 min). The C1-oxidized oligosaccharides were assigned based on standards from previous studies[8,33]. Curves are the average of triplicate experiments.

Abbreviations

Asc: Ascorbic Acid; β-DM:β-D-Maltoside; Chl:Chlorophyll; CNF:Cellulose nanofibrils; CV:Column volumes; EtOH:Ethanol; HPAEC:High-Performance Anion Exchange Chromatography; H$_2$O$_2$:Hydrogen peroxide; LPMO:Lytic polysaccharide monooxygenase; O$_2$:Oxygen; ^{1}O$_2$:Singlet oxygen; O^{2-}:Superoxide; SDS-

PAGE:Sulfate-polyacrylamide gel electrophoresis; SEM:Standard error of the mean. *Tt*AA9:LPMO from *Thielavia terretris*; WSCP:Water-soluble chlorophyll protein.

Declarations

Ethics approval and consent to participate

Not applicable.

Consent for publication

Not applicable.

Competing interests

The authors declare that they have no conflict of interests.

Availability of data and material

All appropriate data for the study has been included in the manuscript.

Funding

Authors' contributions

P.E.J. and D.A.R. conceived this project. N.D and D.A.R. designed experiments. N.D. performed the experiments and analyzed the data. D.A.R. and B.M.B helped to perform the experiments and collect the data. R.K.S., B.V.O., R.C., and M.J.B provided enzymes, and assisted with analyzing data and preparing the manuscript. All authors read and approved the submission of this manuscript.

Acknowledgements

References

1. Correa DF, Beyer HL, Fargione JE, et al. Towards the implementation of sustainable biofuel production systems. *Renew Sustain Energy Rev*. 2019. doi:10.1016/j.rser.2019.03.005

2. Marriott PE, Gómez LD, Mcqueen-Mason SJ. Unlocking the potential of lignocellulosic biomass through plant science. *New Phytol*. 2016. doi:10.1111/nph.13684

3. Lee SH, Choi DS, Kuk SK, Park CB. Photobiocatalysis: Activating Redox Enzymes by Direct or Indirect Transfer of Photoinduced Electrons. *Angew Chemie - Int Ed*. 2018;57(27):7958-7985. doi:10.1002/anie.201710070

4. Maciá-Agulló JA, Corma A, Garcia H. Photobiocatalysis: The Power of Combining Photocatalysis and Enzymes. *Chem - A Eur J*. 2015;21(31):10940-10959. doi:10.1002/chem.201406437

5. Russo DA, Zedler JAZ, Jensen PE. A force awakens: Exploiting solar energy beyond photosynthesis. *J Exp Bot*. 2019. doi:10.1093/jxb/erz054

6. Lassen LM, Nielsen AZ, Ziersen B, Gnanasekaran T, Møller BL, Jensen PE. Redirecting photosynthetic electron flow into light-driven synthesis of alternative products including high-value bioactive natural compounds. *ACS Synth Biol*. 2014;3(1):1-12. doi:10.1021/sb400136

7. Ito H, Kondo R, Yoshimori K, Kamachi T. Methane Hydroxylation with Water as an Electron Donor under Light Irradiation in the Presence of Reconstituted Membranes Containing both Photosystem II and a Methane Monooxygenase. *ChemBioChem*. 2018. doi:10.1002/cbic.201800324

8. Cannella D, Möllers KB, Frigaard N-U, et al. Light-driven oxidation of polysaccharides by photosynthetic pigments and a metalloenzyme. *Nat Commun*. 2016;7(1):1-8. doi:10.1038/ncomms11134

9. Bissaro B, Kommedal E, Røhr ÅK, Eijsink VGH. Controlled depolymerization of cellulose by light-driven lytic polysaccharide oxygenases. *Nat Commun*. 2020. doi:10.1038/s41467-020-14744-9

10. Blossom BM, Russo DA, Singh RK, et al. Photobiocatalysis of a Lytic Polysaccharide Monooxygenases by Sequential Illumination. *ACS Sustain Chem Eng*. 2020;(Manuscript submitted for publication.).

11. Johansen KS. Lytic Polysaccharide Monooxygenases: The Microbial Power Tool for Lignocellulose Degradation. *Trends Plant Sci*. 2016;21(11):926-936. doi:10.1016/j.tplants.2016.07.012

12. Quinlan RJ, Sweeney MD, Lo Leggio L, et al. Insights into the oxidative degradation of cellulose by a copper metalloenzyme that exploits biomass components. *Proc Natl Acad Sci U S A*. 2011. doi:10.1073/pnas.1105776108

13. Müller G, Várnai A, Johansen KS, Eijsink VGH, Horn SJ. Harnessing the potential of LPMO-containing cellulase cocktails poses new demands on processing conditions. *Biotechnol Biofuels*. 2015;8(1):187. doi:10.1186/s13068-015-0376-y

14. Hu J, Chandra R, Arantes V, Gourlay K, Susan van Dyk J, Saddler JN. The addition of accessory enzymes enhances the hydrolytic performance of cellulase enzymes at high solid loadings. *Bioresour Technol*. 2015. doi:10.1016/j.biortech.2015.03.055

15. Hu J, Arantes V, Pribowo A, Gourlay K, Saddler JN. Substrate factors that influence the synergistic interaction of AA9 and cellulases during the enzymatic hydrolysis of biomass. *Energy Environ Sci*.

2014. doi:10.1039/c4ee00891j

16. Kuusk S, Kont R, Kuusk P, et al. Kinetic insights into the role of the reductant in H 2 O 2 -driven degradation of chitin by a bacterial lytic polysaccharide monooxygenase. *J Biol Chem*. 2019;294(5):1516-1528. doi:10.1074/jbc.RA118.006196

17. Bissaro B, Røhr ÅK, Müller G, et al. Oxidative cleavage of polysaccharides by monocopper enzymes depends on H2O2. *Nat Chem Biol*. 2017;13(10):1123-1128. doi:10.1038/nchembio.2470

18. Singh RK, Blossom BM, Russo DA, et al. Detection and Characterization of a Novel Copper-Dependent Intermediate in a Lytic Polysaccharide Monooxygenase. *Chem – A Eur J*. 2020;26(2):454-463. doi:10.1002/chem.201903562

19. Müller G, Chylenski P, Bissaro B, Eijsink VGH, Horn SJ. The impact of hydrogen peroxide supply on LPMO activity and overall saccharification efficiency of a commercial cellulase cocktail. *Biotechnol Biofuels*. 2018;11(1):1-17. doi:10.1186/s13068-018-1199-4

20. Schmermund L, Jurkaš V, Özgen FF, et al. Photo-Biocatalysis: Biotransformations in the Presence of Light. *ACS Catal*. 2019. doi:10.1021/acscatal.9b00656

21. Kwiatkowski S, Knap B, Przystupski D, et al. Photodynamic therapy – mechanisms, photosensitizers and combinations. *Biomed Pharmacother*. 2018. doi:10.1016/j.biopha.2018.07.049

22. Baptista MS, Cadet J, Di Mascio P, et al. Type I and Type II Photosensitized Oxidation Reactions: Guidelines and Mechanistic Pathways. *Photochem Photobiol*. 2017. doi:10.1111/php.12716

23. Schmidt K, Fufezan C, Krieger-Liszkay A, Satoh H, Paulsen H. Recombinant water-soluble chlorophyll protein from Brassica oleracea var. Botrys binds various chlorophyll derivatives. *Biochemistry*. 2003;42(24):7427-7433. doi:10.1021/bi034207r

24. Palm DM, Agostini A, Tenzer S, et al. Water-Soluble Chlorophyll Protein (WSCP) Stably Binds Two or Four Chlorophylls. *Biochemistry*. 2017;56(12):1726-1736. doi:10.1021/acs.biochem.7b00075

25. Yamada K, Hara-Nishimura I, Nishimura M. Unique defense strategy by the endoplasmic reticulum body in plants. *Plant Cell Physiol*. 2011. doi:10.1093/pcp/pcr156

26. Takahashi S, Yanai H, Nakamaru Y, Uchida A, Nakayama K, Satoh H. Molecular cloning, characterization and analysis of the intracellular localization of a water-soluble chl-binding protein from brussels sprouts (brassica oleracea var. gemmifera). *Plant Cell Physiol*. 2012. doi:10.1093/pcp/pcs031

27. Agostini A, Palm DM, Schmitt FJ, et al. An unusual role for the phytyl chains in the photoprotection of the chlorophylls bound to Water-Soluble Chlorophyll-binding Proteins. *Sci Rep*. 2017;7(1):1-13. doi:10.1038/s41598-017-07874-6

28. Bryksin A V., Matsumura I. Overlap extension PCR cloning: A simple and reliable way to create recombinant plasmids. *Biotechniques*. 2010. doi:10.2144/000113418

29. Gasteiger E, Hoogland C, Gattiker A, et al. Protein Identification and Analysis Tools on the ExPASy Server. In: *The Proteomics Protocols Handbook*. ; 2005. doi:10.1385/1-59259-890-0:571

30. Singh RK, Blossom BM, Russo DA, et al. Thermal unfolding and refolding of a lytic polysaccharide monooxygenase from: Thermoascus aurantiacus. *RSC Adv*. 2019. doi:10.1039/c9ra05920b

31. Keller MB, Felby C, Labate CA, et al. A simple enzymatic assay for the quantification of C1-specific cellulose oxidation by lytic polysaccharide monooxygenases. *Biotechnol Lett*. 2020. doi:10.1007/s10529-019-02760-9

32. Westereng B, Agger JW, Horn SJ, et al. Efficient separation of oxidized cello-oligosaccharides generated by cellulose degrading lytic polysaccharide monooxygenases. *J Chromatogr A*. 2013. doi:10.1016/j.chroma.2012.11.048

33. Möllers KB, Mikkelsen H, Simonsen TI, et al. On the formation and role of reactive oxygen species in light-driven LPMO oxidation of phosphoric acid swollen cellulose. *Carbohydr Res*. 2017;448:182-186. doi:10.1016/j.carres.2017.03.013

34. Zhang R, Liu Y, Zhang Y, et al. Identification of a thermostable fungal lytic polysaccharide monooxygenase and evaluation of its effect on lignocellulosic degradation. *Appl Microbiol Biotechnol*. 2019. doi:10.1007/s00253-019-09928-3

35. Hu J, Tian D, Renneckar S, Saddler JN. Enzyme mediated nanofibrillation of cellulose by the synergistic actions of an endoglucanase, lytic polysaccharide monooxygenase (LPMO) and xylanase. *Sci Rep*. 2018. doi:10.1038/s41598-018-21016-6

36. Zhang Y, Yang J, Luo L, et al. Low-cost cellulase-hemicellulase mixture secreted by Trichoderma harzianum EM0925 with complete saccharification efficacy of lignocellulose. *Int J Mol Sci*. 2020. doi:10.3390/ijms21020371

37. Koca N, Karadeniz F, Burdurlu HS. Effect of pH on chlorophyll degradation and colour loss in blanched green peas. *Food Chem*. 2007. doi:10.1016/j.foodchem.2005.09.079

38. Gerola AP, Tsubone TM, Santana A, De Oliveira HPM, Hioka N, Caetano W. Properties of chlorophyll and derivatives in homogeneous and microheterogeneous systems. *J Phys Chem B*. 2011. doi:10.1021/jp201278b

39. Monooxygenase P. pH-Dependent Relationship between Catalytic Activity and Hydrogen Peroxide Production Shown via Characterization of. *Appl Environ Microbiol*. 2019;85(5):1-15.

40. Eijsink VGH, Petrovic D, Forsberg Z, et al. On the functional characterization of lytic polysaccharide monooxygenases (LPMOs). *Biotechnol Biofuels*. 2019;12(1):1-16. doi:10.1186/s13068-019-1392-0

41. Chylenski P, Bissaro B, Sørlie M, et al. Lytic Polysaccharide Monooxygenases in Enzymatic Processing of Lignocellulosic Biomass. *ACS Catal*. 2019;9(6):4970-4991. doi:10.1021/acscatal.9b00246

42. Kramarenko GG, Hummel SG, Martin SM, Buettner GR. Ascorbate Reacts with Singlet Oxygen to Produce Hydrogen Peroxide. *Photochem Photobiol*. 2006;82(6):1634-1637. doi:10.1562/2006-01-12-RN-774

43. Monooxygenase P. pH-Dependent Relationship between Catalytic Activity and Hydrogen Peroxide Production Shown via Characterization of. *Appl Environ Microbiol*. 2019.

44. Deutsch JC. Ascorbic acid oxidation by hydrogen peroxide. *Anal Biochem*. 1998. doi:10.1006/abio.1997.2293

45. Dewhirst RA, Fry SC. The oxidation of dehydroascorbic acid and 2,3-diketogulonate by distinct reactive oxygen species. *Biochem J*. 2018. doi:10.1042/BCJ20180688

46. Hegnar OA, Petrovic DM, Bissaro B, Alfredsen G, Várnai A, Eijsink VGH. pH-Dependent Relationship between Catalytic Activity and Hydrogen Peroxide Production Shown via Characterization of a Lytic Polysaccharide Monooxygenase from Gloeophyllum trabeum. Master ER, ed. *Appl Environ Microbiol*. 2018;85(5). doi:10.1128/AEM.02612-18

47. Aphalo PJ, Albert A, Björn LO, McLeod AR, Robson TM, Rosenqvist E. *Beyond the Visible: A Handbook of Best Practice in Plant UV Photobiology*. University of Helsinki, Department of Biosciences; 2012. doi:10.31885/9789521083631
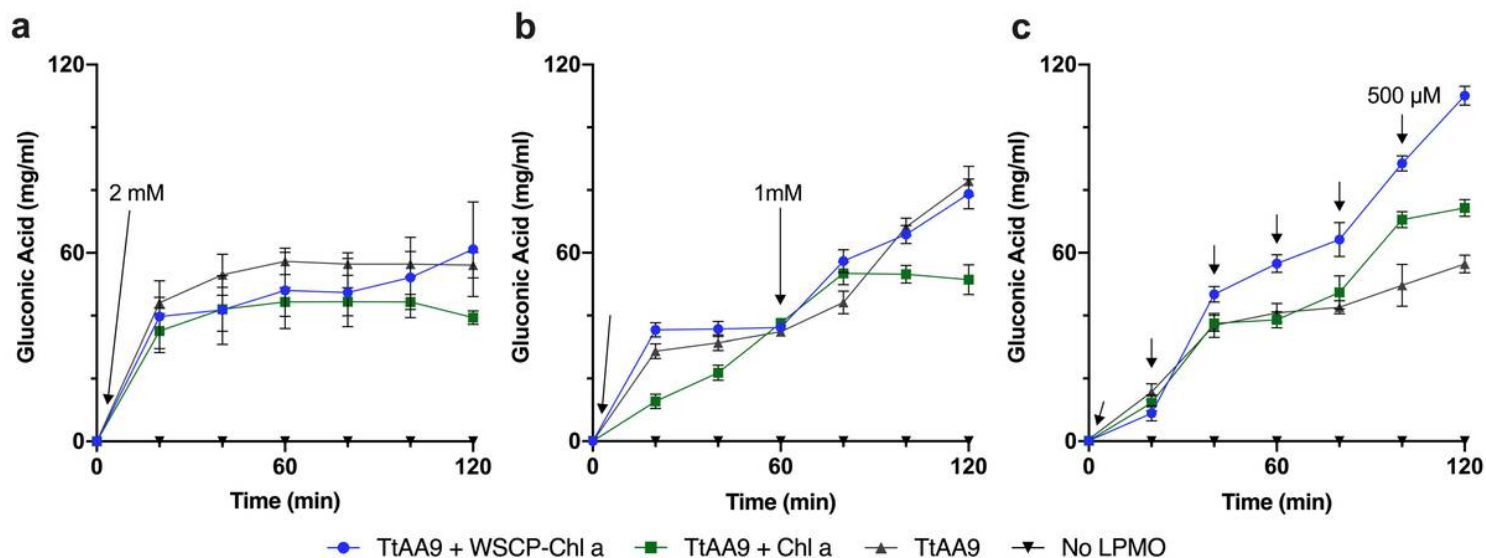
Figures
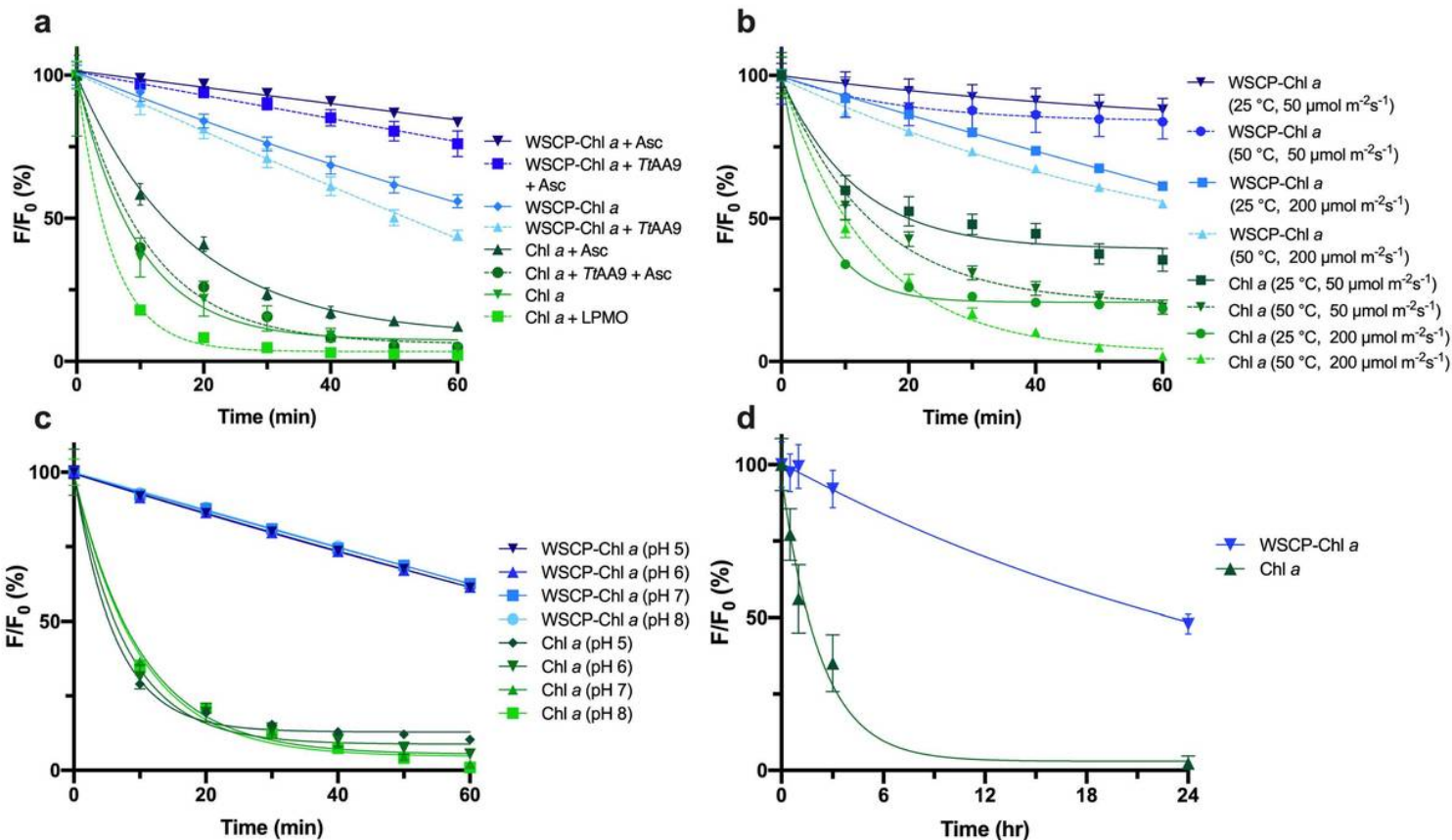
Figure 1

Photostability of WSCP-Chl a and free Chl a. Fluorescence measured every 10 min (F) is divided by starting fluorescence (F0) to show the loss over time. Blue lines represent WSCP-Chl a complexes (2.6 µM) and green lines represent free Chl a (2.6 µM) in 0.03 % ß-DM. Curves are averages of three independent experiments and the standard error of each. (a) Comparing the effect of LPMO activity assay components on the stability of WSCP-Chl a and free Chl a. Assay components were in the following concentrations: Asc (1mM), TtAA9 (0.035 mg mL-1), buffer (pH 6.3). Conditions: 25 °C and 500 µmol m-2 s-1. (b) WSCP-Chl a and Chl a under different light and temperature conditions (25°C/50°C; 0-200 µmol m-2 s-1) and contained pigments (2.6 µM) and buffer (pH 6.3). (c) Photostability of WSCP-Chl a and Chl a at different pH. Assay composed of pigments (2.6 µM) and buffer (pH 5-8). Conditions: 25 °C and 500 µmol m-2 s-1. (d) 24-hour photostability assay performed at 50 µmol m-2 s-1 with pigments (2.6 µM) and buffer (pH 6.3). All assays were performed with cool white LEDs (4000K) spectrum.
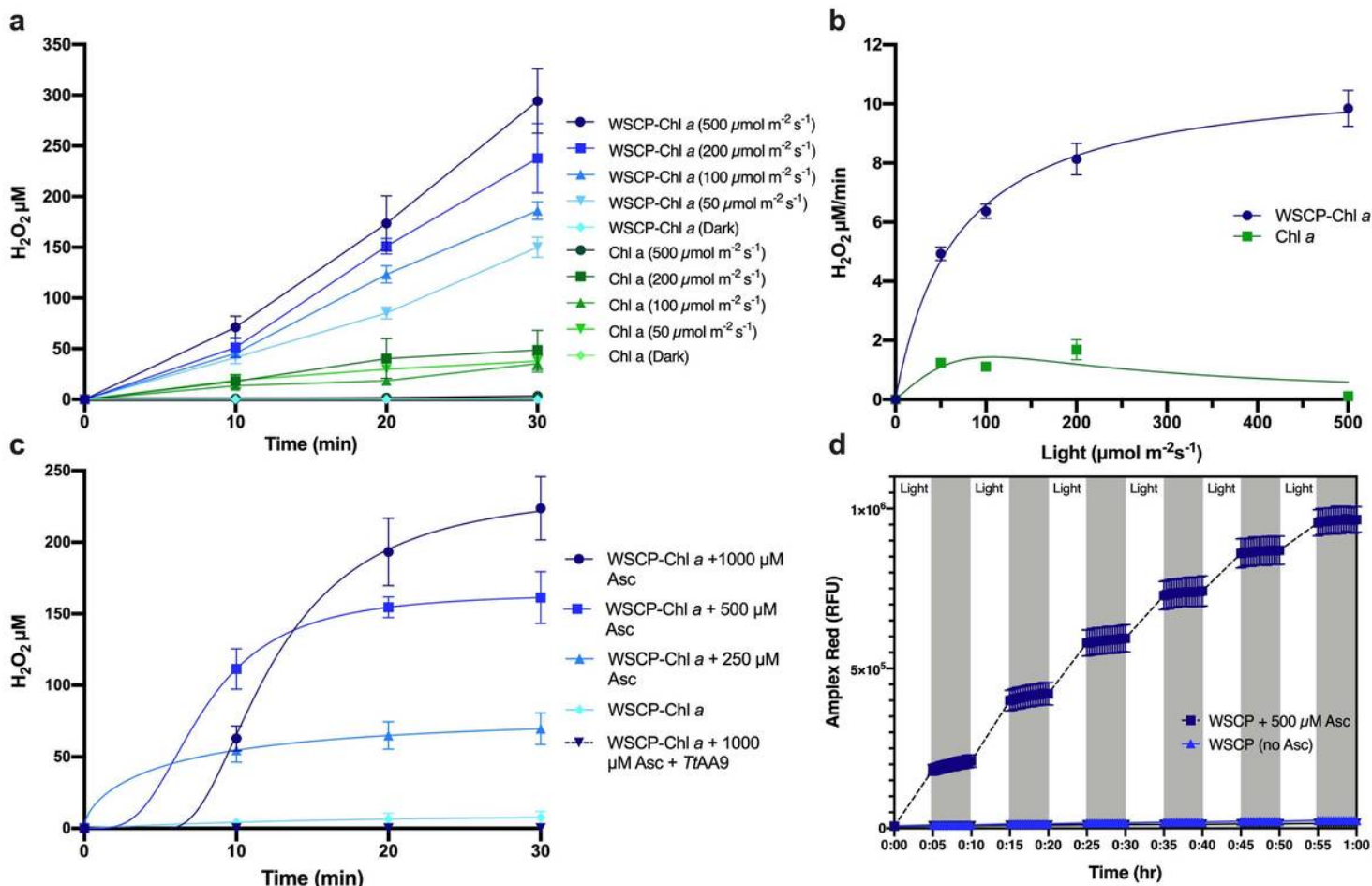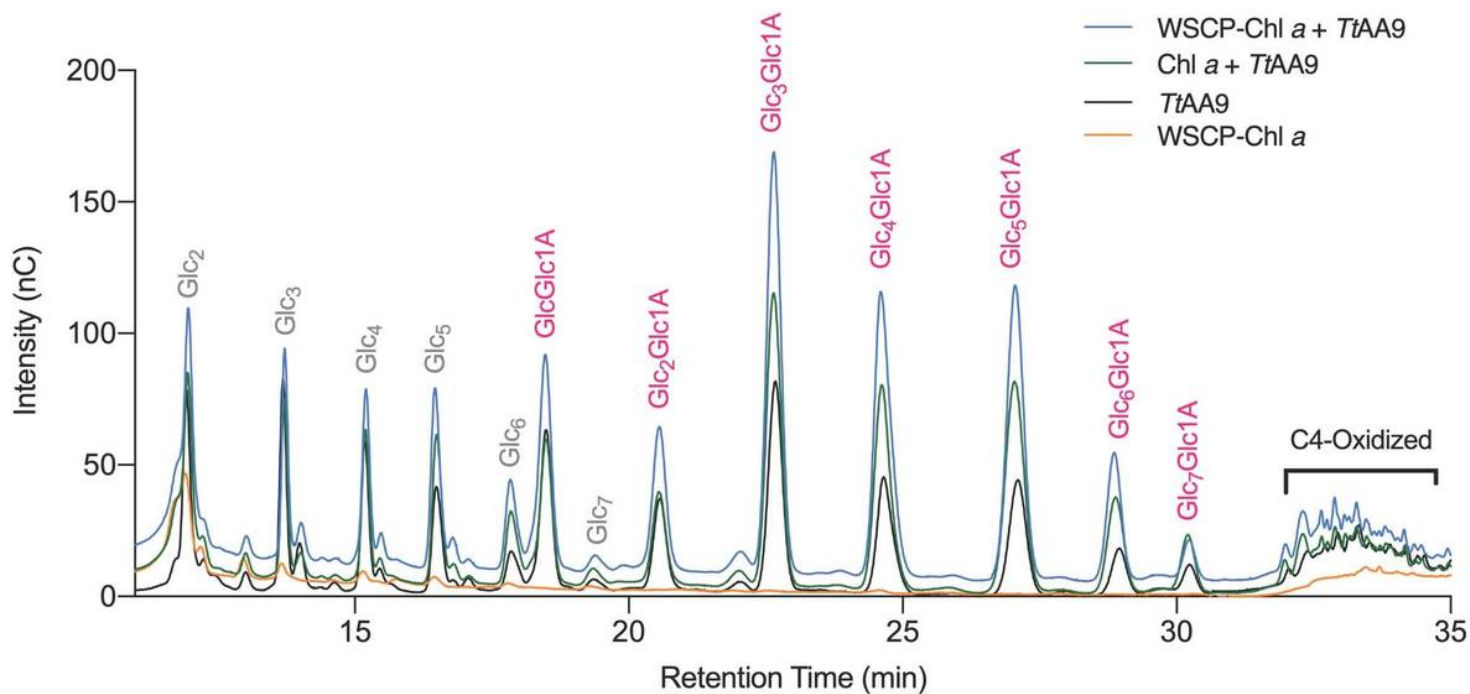
Figure 2

Light dependent H2O2 formation of WSCP-Chl a under different conditions. Using an Ampliflu™ assay, H2O2 accumulation was measured under different conditions. Blue lines represent WSCP-Chl a complexes and green lines represent unbound Chl a in 0.03 % ß-DM. Each point is the average of three independent experiments and the corresponding SEM. Light assay components were in the following concentrations: pigments (2.6 μM), and 50 mM potassium phosphate buffer (pH 6.3). (a) Five different light intensities were tested: 500, 200, 100, 50, and 0 (dark control) μmol m-2 s-1 cool white light (4000K) spectrum. Assays composed of: pigments (2.6 μM), Asc (1 mM), and 50 mM sodium phosphate buffer (pH 6.3). (b) Rate constants of H2O2 formation at different light intensities calculated from each curve under the 5 light intensities (0, 50, 100, 200, 500 μmol m-2 s-1) for both WSCP-Chl a and unbound Chl a. (c) Five different conditions were tested with WSCP-Chl a: 1000, 500, 250, 0μM Asc and 1000 μM Asc + TtAA9. The TtAA9 (0.035 mg mL-1) and CNF (0.25% w/v). Light intensity was set to 500 μmol m-2s-1. The final H2O2 concentration (30 min) was analyzed with single factor ANOVA for all WSCP-Chl a samples (not including the LPMO control). (d) Light/dark accumulation of H2O2 with WSCP-Chl a in the presence and absence of Asc, alternating between 5 min in the 50 μmol m-2 s-1 followed by 5 min of fluorescence measurements in the dark.
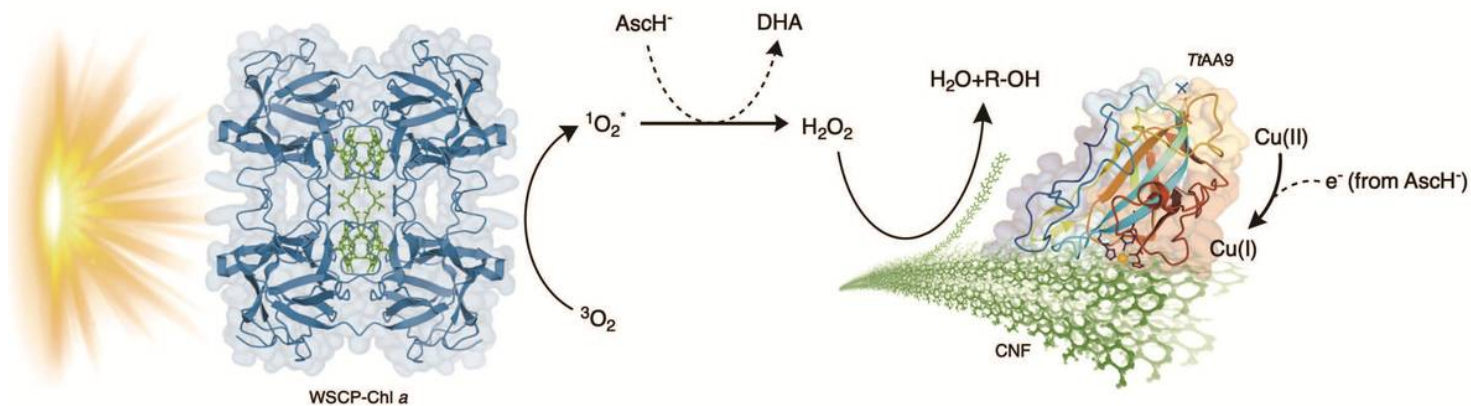
Figure 3

Gluconic acid determination after light driven TtAA9 time course assays under various Asc feed rates. All three assays were performed at 100 µmol m-2 s-1 cool white LED (4000K) spectrum at 25°C in 50 mM potassium phosphate buffer (pH 6.3), with CNF (0.25 % w/v) and either TtAA9 and WSCP-Chl a, TtAA9 and Chl a, TtAA9 without pigment, or WSCP-Chl a as a no enzyme control. Asc feed rates were: (a) 2 mM Asc, (b) 1mM Asc/hour, or (c) 500 µM every 20 min. Curves are averages of three independent experiments and the SEM of these experiments is shown. Single factor ANOVA was done on the final gluconic acid concentration (120 min) between TtAA9 w/ and w/o WSCP-Chl a.

Figure 4

HPAEC Chromatograms of TtAA9 with WSCP-Chl a, TtAA9 with Chl a, TtAA9 without any pigments, and WSCP-Chl a control without TtAA9. These were taken after 3 h at 50 µmol m-2 s-1 and 50 °C with 50 mM potassium phosphate buffer (pH 6), with CNF (0.25 % w/v) and 500 µM Asc/h. Peaks were assigned based on standards: cellobiose (Glc2), cellotriose (Glc3), cellotetraose (Glc4), cellopentaose (Glc5), cellohexaose (Glc6), and celloheptaose (Glc7). C1-oxidized oligosaccharides (pink) are cellobionic acid (GlcGlc1A), cellotrionic acid (Glc2Glc1A), cellotetraonic acid (Glc3Glc1A), cellopentaoinic acid (Glc4Glc1A), cellohexaoinic acid (Glc5Glc1A), celloeptaonic acid (Glc6Glc1A), and cellooctaonic acid (Glc7Glc1A).

Figure 5

Proposed ROS-mediated light-driven enhancement of TtAA9 with WSCP-Chl a. Triplet excited Chl a transfer excitation energy to 3O2 forming 1O2* upon light exposure. In the presence of AscH-, 1O2 * is reduced to H2O2 which can be used by a reduced Cu(I)-TtAA9 for hydrolysis of CNF. TtAA9 (PDB: 3EJA), WSCP1 tetramer reconstituted with Chl. (PDB: 6S2Z).

Supplementary Files

This is a list of supplementary files associated with this preprint. Click to download.

- SupplementaryFigures.docx